Infrared Interference Thickness Inversion Based on Hilbert Analytic Signal and Full-Spectrum Phase Regression

Ruiqian Huang †, Hongrui Zhong † and Chenxi Yang †, *

South China Normal University, Guangzhou, China

* Corresponding Author Email: 3534315041@qq.com

† These authors also contributed equally to this work

Abstract. This paper proposes a unified algorithmic framework that integrates physical modeling and signal processing for the stable extraction of interference fringe information and the inversion of epitaxial layer thickness in infrared reflectance spectroscopy. First, an optical interference model is established based on phase difference theory, explicitly linking the thickness parameter to the phase-wavenumber relationship, and unifying the description of model parameters through a refractive index correction term. At the signal processing level, Savitzky–Golay filtering is employed for baseline subtraction, and the Hilbert transform is utilized to construct an analytical signal, thereby separating the amplitude and phase of the interference signal and converting the original oscillatory structure into a continuous phase representation. Building on this, phase expansion and linear fitting methods are introduced to propose a full-spectrum phase regression model, transforming the thickness estimation into a global parameter solving problem and thereby reducing dependence on local features. Furthermore, a dual-path inversion mechanism is constructed by combining extreme value spacing calculation methods, and the stability of the results is enhanced through statistical averaging of multiple sets of fringes. Concurrently, a multi-beam interference expansion expression based on the Airy model is introduced, enabling the algorithm to maintain a consistent computational form under varying reflection conditions. Experimental results demonstrate that this method exhibits excellent numerical consistency and noise resistance under diverse data conditions, and the overall framework possesses strong versatility and scalability.

Keywords: Hilbert Analytic Signal; Full-Spectrum Phase Regression; Savitzky–Golay Filtering.

1. Introduction

Infrared reflectance spectroscopy offers advantages such as non-contact measurement and high resolution in the characterization of thin-film structural parameters, with the phase information carried by interference fringes being key to thickness inversion [1]. However, in practical measurements, spectral signals are often superimposed with low-frequency background and high-frequency noise, causing the fringe structure to deviate from the ideal state, which directly affects the stability and accuracy of the inversion results. Furthermore, traditional methods often rely on fringe extrema or local features, making them sensitive to signal quality. Under complex interference conditions, these methods are prone to fluctuations, making it difficult to establish a unified and robust solution path [2].

Therefore, it is necessary to construct a comprehensive algorithmic framework that integrates physical modeling and signal processing. This paper treats phase as the core intermediate variable. Through signal decomposition and phase expansion, it transforms the problem—which originally relied on the identification of periodic structures—into a continuous function fitting problem, thereby reducing dependence on local features. Building on this foundation, a dual-path inversion strategy and a multi-beam expansion model are introduced, enabling the method to adapt to complex reflection conditions while maintaining computational simplicity [3].

This framework maintains a unified form in model representation and emphasizes the utilization of global information during the solution process, demonstrating excellent stability and scalability. Taking a silicon carbide epitaxial layer as an example, the proposed method achieves stable inversion

of thickness parameters in real spectral data, validating its application potential in thin-film measurement.

2. Optical Interference Phase Modeling and Parameter Representation Methods

2.1. Phase Difference Modeling

The key point of infrared interference measurement is not the fringes themselves, but the phase information represented by these fringes. For the silicon carbide epitaxial layer, under the simplified condition of "single reflection + transmission", the interference mainly comes from the superposition of two coherent light beams.

One beam is directly reflected at the surface of the epitaxial layer, while the other enters the epitaxial layer, is reflected at the substrate interface, and then exits again. Since the two beams come from the same light source, they have the same frequency and a stable phase relationship, which produces periodic interference fringes. These fringes are not randomly distributed. Their positions are determined by the phase difference between the two beams, and this phase difference is directly controlled by the thickness of the epitaxial layer.

The phase difference mainly consists of two parts: one is the optical path difference caused by light propagation inside the epitaxial layer, and the other is the phase change caused by interface reflection. Together, it can be written as:

$$\Delta\psi = \frac{4\pi nd\cos\theta}{\lambda} + \Delta\psi_2 \tag{1}$$

Where n is the refractive index of the epitaxial layer, d is the thickness, θ is the refraction angle, λ is the incident wavelength, and $\Delta\psi_2$ denotes the interface phase term.

The interference fringes satisfy the phase condition: $\Delta\psi = 2m\pi$ or $(2m+1)\pi$.

This relation has already built a connection between the thickness and the measurable fringes. The fringe positions can be regarded as discrete samples of the phase in the wavenumber space, and the thickness information is reflected through these sampling points.

2.2. Refraction and Optical Path

The refraction angle is one of the important factors affecting the phase difference, as it determines the actual propagation path of light in the epitaxial layer. The derivation is not expanded here, and only the necessary relation is retained: the incident angle and the refraction angle satisfy Snell's law, so the refraction angle can be directly calculated from the incident angle and the refractive index.

The advantage of this treatment is that the propagation path problem can be uniformly transformed into a functional relationship between thickness and refractive index, avoiding the introduction of additional unknown variables.

It should be noted that this model assumes that the epitaxial layer is a uniform plane-parallel thin film. If the thickness distribution is uneven or the interface is not flat, the optical path difference at different positions will change, and the interference fringes will lose their stability accordingly. This point needs special attention in practical applications.

2.3. Refractive Index Modeling

The refractive index of the epitaxial layer varies with wavelength and carrier concentration, so it should not simply be treated as a constant. For ease of calculation, a unified expression is used here:

$$n_e = \sqrt{n^2(\lambda) + \Delta n^2} \tag{2}$$

Where $n(\lambda)$ represents the intrinsic refractive index, and Δn^2 represents the correction term caused by carriers. This form avoids complicated expansion while maintaining sufficient accuracy, making it suitable for later numerical calculation.

2.4. Thickness Estimation Model

After the phase relation and the refractive index are determined, the thickness can be obtained by inversion from the interference fringes. Compared with directly using the phase expression, using the wavenumber difference between adjacent fringes is more stable. According to the interference relation:

$$d = \frac{1}{2n\Delta\tilde{\nu}\cos\theta} \tag{3}$$

Where $\Delta\tilde{\nu}$ is the wavenumber difference between adjacent fringes.

Considering fluctuations in actual data, multiple groups of fringe-based results are usually selected and averaged:

$$\tilde{d} = \frac{1}{k}\sum d_i \tag{4}$$

This treatment can effectively reduce random errors and make the result more stable. At this point, the model has moved from a purely physical relation to a form that can be directly used for data calculation.

3. Spectral Signal Processing Framework for Phase Extraction

3.1. Spectral Characteristics

For the infrared reflection spectrum of the silicon carbide epitaxial layer, the measured spectrum is not an ideal interference fringe pattern, but a composite signal formed by the superposition of multiple components. It mainly includes periodic interference fringes, low-frequency background components, and high-frequency noise.

The low-frequency part usually comes from the light source distribution, detector response, and sample surface condition, which shifts the overall baseline. The high-frequency components mainly arise from measurement noise and environmental disturbances. If these factors are not handled, they will directly affect the identification of the fringe structure and then reduce the stability of thickness inversion.

Therefore, before phase extraction, the original signal needs to be separated to highlight the main structure of the interference fringes.

3.2. Baseline Removal

For the low-frequency background, a Savitzky–Golay (S-G) filter is used to extract the slowly varying trend, and this baseline is subtracted from the original signal. This gives a signal dominated by interference fringes [4].

After baseline removal, the periodic structure of the fringe becomes more pronounced, which is helpful for later phase extraction. This step is simple, but it has a noticeable impact on the overall result. Improper processing here can lead to instability in the subsequent calculations.

3.3. Analytic Signal Construction

After obtaining the fringe signal, the phase information still needs to be extracted. Since directly reading the phase from an oscillatory signal is sensitive to phase wrapping, the Hilbert transform is used to construct the analytic signal:

$$z(\sigma) = R_s(\sigma) + iH[R_s] \tag{5}$$

Where $R_s(\sigma)$ is the signal after baseline removal.

In this representation, the amplitude corresponds to the fringe intensity, while the phase corresponds to the interference phase. The reflectance can be written as:

$$R = A + B\cos(\Delta\phi) \tag{6}$$

This form separates the original oscillatory signal into amplitude and phase components, so the phase information can be directly used in later calculations.

3.4. Phase Extraction and Enhancement

Based on the analytic signal, after applying phase unwrapping, a relatively smooth phase curve can be obtained, as shown in Fig. 1.

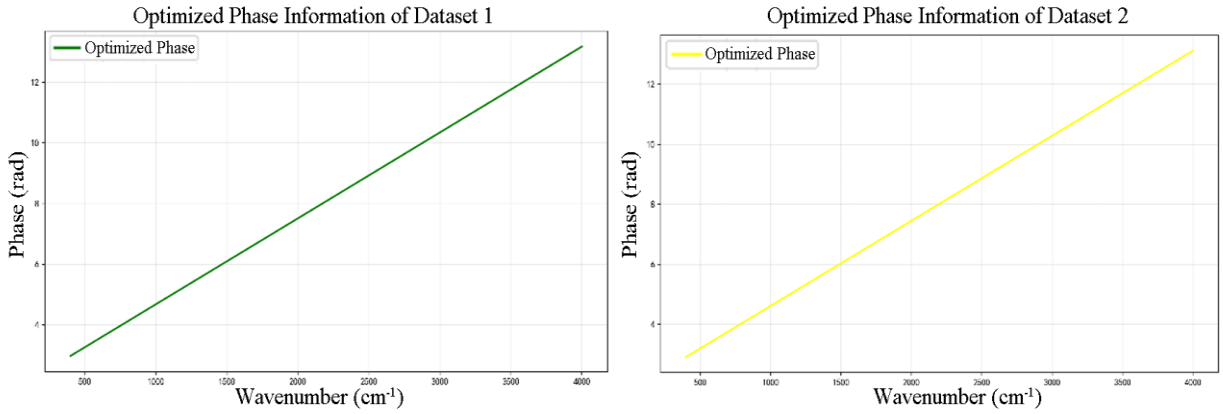

Fig 1. Two or more references.

It can be observed that there is a clear linear relationship between the phase and the wavenumber. This feature turns the problem, which originally depends on periodic structures, into a linear fitting problem, providing a more stable path for thickness inversion.

4. Thickness Inversion Algorithms Based on Dual-Strategy Methods

The goal of thickness inversion is to convert the structural information in the interference fringes into the thickness of the epitaxial layer. Based on the phase modeling and signal processing results above, two strategies are used here: one based on fringe spacing, and the other based on the overall phase trend. The two methods focus on different aspects, but both point to the same physical quantity.

4.1. Extremum-Based Thickness Estimation

This method makes use of the periodic nature of the interference fringes and estimates the thickness from the spacing between adjacent extrema.

After preprocessing, the extrema of the fringes can be identified in a stable way. By sorting these extrema in wavenumbers, the wavenumber difference between adjacent fringes $\Delta\tilde{\nu}$ can be obtained. According to the interference relation:

$$d = \frac{1}{2n\Delta\tilde{\nu}\cos\theta} \tag{7}$$

This expression turns the phase problem into a spacing calculation between fringes, which is more direct.

Considering possible errors in extremum detection, multiple groups of adjacent fringes are usually selected, and the results are average:

$$\tilde{d} = \frac{1}{k}\sum d_i \tag{8}$$

This method is simple to implement, but it is quite sensitive to fringe quality. When the fringes are not clear or the noise is strong, the result tends to fluctuate.

4.2. Full-Spectrum Phase Regression

The full-spectrum phase regression method uses the phase information over the entire spectrum to estimate the thickness.

Based on the analytic signal obtained in Section 3, the phase ϕ can be extracted continuously. It shows an approximately linear relationship with the wavenumber:

$$\phi(f) = 4\pi nd \cdot f + \Delta\phi_0 \tag{9}$$

Where the slope is related to the thickness, and the intercept corresponds to the interface phase term.

By performing a linear fit on the "phase–wavenumber" data, the slope k is obtained, and the thickness can be directly calculated as:

$$d = \frac{k}{4\pi n} \tag{10}$$

This method uses the full set of data for fitting, so it is less sensitive to local noise and shows better overall stability. When the fringe quality is poor or disturbances are present, it usually performs better than the extremum-based method.

5. Airy-Based Multi-Beam Interference Modeling Method

5.1. Conditions for Multi-Beam Interference

The previous model is based on the two-beam interference assumption. In actual measurements, however, light inside the epitaxial layer often undergoes multiple reflections, leading to multi-beam interference effects.

When the epitaxial layer is uniform and the interface reflectivity is moderate, the multiple reflected beams can maintain stable phase relationships and take part in the superposition. As a result, the interference fringes show higher contrast and sharper peak–valley features [5].

The formation of multi-beam interference is mainly constrained by the following factors:

(1) Structural condition: the epitaxial layer should be close to a plane-parallel thin film, and the thickness distribution needs to remain uniform, so that the optical path difference stays stable;

(2) Reflection condition: the interface reflectivity should be in a moderate range. If the reflectivity is too high, the fringes become too narrow and harder to identify reliably; if it is too low, higher-order reflections can be neglected, and the system reduces to two-beam interference;

(3) Source condition: the incident light should be approximately monochromatic and well-directed, in order to maintain phase consistency.

These conditions together determine whether multi-beam interference is significant. If they are not satisfied, the effect of multiple reflections on the interference structure can be neglected.

5.2. Airy-Based Multi-Beam Model

Under multi-beam interference conditions, a more complete model is needed to describe the intensity distribution. The Airy model is used here, and the reflectance is written as [6]:

$$R = \frac{R_{01} + R_{12} + 2\sqrt{R_{01}R_{12}}\cos\Delta\phi}{1 + R_{01}R_{12} + 2\sqrt{R_{01}R_{12}}\cos\Delta\phi} \tag{11}$$

Where R_{01} and R_{12} are the reflectivities of the upper and lower interfaces, and $\Delta\phi$ is the phase difference.

The phase still satisfies:

$$\Delta\phi = 4\pi nd\cos\theta \cdot \nu \tag{12}$$

It can be seen that the multi-beam model extends the expression of reflectance, while the thickness still enters the model through the phase term. Therefore, the phase extraction methods described earlier remain applicable in this case.

5.3. Model Mismatch and Accuracy Implications

The choice of model has a direct impact on the thickness calculation.

If multi-beam interference is present in reality but a two-beam model is used, the phase condition will shift, introducing a systematic error. This error increases with the interface reflectivity.

On the other hand, multi-beam interference makes the fringes sharper, which helps improve the accuracy of extremum localization, but it also increases sensitivity to noise. When the signal quality is low, this may reduce the stability of the result.

Therefore, model suitability matters more than model complexity. If the data characteristics are closer to two-beam interference, directly applying a multi-beam model may introduce additional errors.

Overall, a reasonable approach is to first determine the type of interference and then choose the corresponding model for thickness inversion.

6. Algorithm Validation and Model Comparison Analysis

This section analyzes the results from four aspects: thickness estimation, consistency validation, comparison with the multi-beam model, and model correction.

6.1. SiC Thickness Estimation Results

After spectral preprocessing and phase extraction, the thickness of the silicon carbide epitaxial layers in Dataset 1 and Dataset 2 is estimated. According to the refractive index model, the variation of refractive index with wavenumber is small, so the average value $n_e = 2.7218$ is used as the calculation parameter.

Within the wavenumber range of 399.67–4000.12 cm^{-1} and with fringe group number $k = 7$, extremum detection is performed. A total of 13 and 12 valid extrema is identified in the two datasets, respectively, indicating that the fringe structure shows good periodicity.

The thickness results obtained from the extremum-based method and the full-spectrum phase regression method are listed in Table 1. The extremum-based result is 8.346 μm, while the full-spectrum phase regression result is about 8.21 μm. The two results are close, suggesting good consistency of the model across different datasets.

Table 1. Required parameters and thickness results.

Parameter	Dataset 1	Dataset 2
n_e	2.7218	2.7218
Fringe group number	7	7
$\tilde{d}_1$	8.346	8.346
$\tilde{d}_2$	8.214	8.216

Compared with the extremum-based method, the full-spectrum method shows better stability, which is further reflected in the following validation.

6.2. Spectral Reconstruction Validation

To check the reliability of the thickness inversion, the estimated thickness is substituted back into the phase model to reconstruct the reflection spectrum, which is then compared with the original measured data.

As shown in Fig. 2, the reconstructed spectrum matches the original spectrum in the main oscillation periods, indicating that the model captures the interference structure well. Local deviations mainly come from noise and deviations of interface conditions from the ideal assumptions.

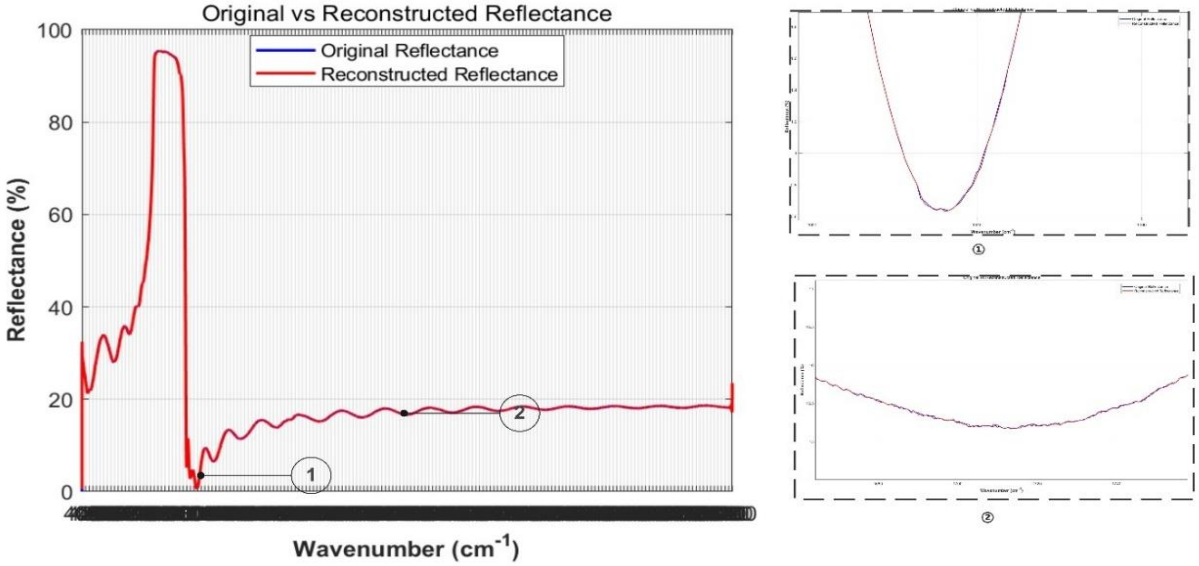

Fig 2. Reflectance before and after reconstruction.

6.3. Silicon Wafer Results under Multi-Beam Model

To examine the applicability of the multi-beam model, the silicon epitaxial layer data in Dataset 3 and Dataset 4 are analyzed. Both the two-beam model and the multi-beam model are applied, with the same full-spectrum phase regression method.

The results are shown in Table 2.

Table 2. Comparison of calculation results.

Metric	Dataset 3 (Two-beam)	Dataset 3 (Multi-beam)	Dataset 4 (Two-beam)	Dataset 4 (Multi-beam)
Thickness	7.488	8.625	7.466	8.615
RSS	137.11	107.35	172.33	135.46
RSS ratio	1.28		1.27	

The multi-beam model significantly reduces the RSS in both datasets, indicating a better fit to the experimental spectra.

The corresponding residual comparison is shown in Fig. 3. The multi-beam model performs better than the two-beam model in fitting both peak–valley positions and periodicity, suggesting that noticeable multiple reflection effects are present in the silicon samples.

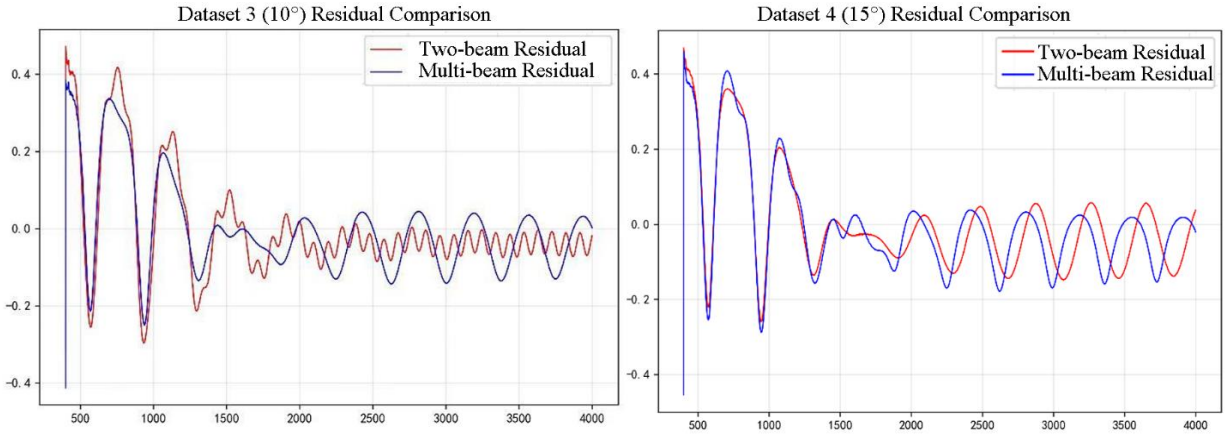

Fig 3. Graph of residual comparison results.

6.4. SiC Model Correction and Comparison

Based on the validation results from the silicon epitaxial layers, model correction is applied to the silicon carbide data. The results are shown in Table 3.

Table 3. Comparison before and after model correction.

Metric	Dataset 1 (Two-beam)	Dataset 1 (Multi-beam)	Dataset 2 (Two-beam)	Dataset 2 (Multi-beam)
Thickness	8.346	7.313	8.346	7.467
RSS	231.31	222.60	269.49	259.48
RSS ratio	1.04		1.04	

The multi-beam model also reduces the RSS here, but the improvement is relatively small (about 4%). This indicates that in the silicon carbide samples, the multi-beam effect is weaker, and the two-beam model already captures the main interference structure.

Overall, the two-beam model is suitable for quick estimation, while the multi-beam model is more appropriate for refined correction when multiple reflection effects are clearly present.

7. Conclusion

This paper addresses the problem of structural parameter inversion in infrared interferometric spectroscopy by developing an integrated algorithmic framework comprising a physical model, signal separation, and phase-driven solution. Based on a unified phase representation, a stable mapping from oscillatory signals to the continuous parameter space is achieved through analytical signal construction and full-spectrum phase regression, combined with an extremum spacing method to form a complementary verification mechanism. Experimental results demonstrate that thickness inversion results maintain good consistency under various data conditions. For example, the results obtained by the two methods are approximately 8.346 μm and 8.21 μm, respectively, with the error controlled within a narrow range, reflecting high computational reliability. Additionally, the introduction of a multi-beam model effectively reduces residuals in certain datasets, indicating that the constructed framework possesses a certain degree of model extensibility.

From a methodological perspective, this study achieves systematic integration from physical constraints to algorithmic implementation, enhancing the model's applicability and stability, and providing valuable reference for the measurement of thin-film structural parameters. Future research could further expand in the direction of complex structures, multi-parameter coupling, and real-time processing to enhance the method's adaptability and engineering applicability.

References

[1] Shentu Xianzhong. Model Transfer for Near-Infrared Spectrometers: Challenges and Strategies Across Instruments and Sample Types [J]. Standardization and Metrology of Instruments and Meters, 2024, (05): 1–3.

[2] Ye Zhen, Bai Lin, He Mingyi. A Review of Spatial and Spectral Feature Extraction in Hyperspectral Images [J]. Chinese Journal of Image and Graphics, 2021, 26(08): 1737-1763.

[3] Zhang Chi, Zou Ningmu, Song Jinyu, et al. Digital Signal Processing and Applications of Φ-OTDR Systems [J]. Opto-Electronics Engineering, 2023, 50(02): 3-21.

[4] Ye Yan, Ma Yaqi, Song Zhi, et al. Dynamic Multi-beam Interferometric Lithography Based on a Fourier Transform Optical System [J]. Acta Optica Sinica, 2023, 43(08): 273-285.

[5] Guan Li. Research on Feature Extraction and Classification Techniques for Hyperspectral Images [D]. Nanjing University of Science and Technology, 2021. DOI: 10.27241/d. cnki. gnjgu. 2021.003452.

[6] Li Weiping, He Jing, Zeng Xiangping, et al. Analysis of Atmospheric Electric Field Signals in Thunderstorm Weather Based on Savitzky-Golay Filtering [J]. Microcomputer Applications, 2023, 39(10): 14-17.